Artifacts caused by insufficient contrast medium filling during C-arm cone-beam CT scans: a phantom study

doi: 10.1007/s12194-013-0227-0

Artifacts caused by insufficient contrast medium filling during C-arm cone-beam CT scans: A phantom study

Mitsuaki Terabe[1,2]**, Hajime Ichikawa**[2]**, Toyohiro Kato**[2]**, and Kichiro Koshida**[1]

[1]Division of Health Sciences, Graduate School of Medical Science, Kanazawa University, 5-11-80, Kodatsuno, Kanazawa, Ishikawa 920-0942, Japan

[2]Department of Radiology, Toyohashi Municipal Hospital, 50, Hakken-nishi, Aotake, Toyohashi, Aichi, 441-8570, Japan

Corresponding author

Mitsuaki Terabe

E-mail: mi.terabe@gmail.com

Tel: 81-532-33-6111

Keywords

C-arm cone-beam computed tomography, contrast medium, DynaCT, angiography

Abstract

We investigated artifacts due to late-arriving contrast medium (CM) during C-arm cone-beam computed tomography. We scanned a phantom filled with water or with 100, 50, or 5% v/v concentrations of CM and then virtually produced CM-delayed projection data by partially replacing the projection images. Artifacts as a function of concentration, percentage of filling time, and size and position of the filling area were assessed. In addition, we used an automatic power injector with different injection delays to inject CM during the scans. A decrease in filling times caused by a lag in CM arrival during the scan resulted in a decrease in pixel values, distortion of the filling area, and appearance of streak artifacts. Even a delay of approximately 20% in CM arrival in the total scan time resulted in obvious distortion of the filling area. The distortion and streak artifacts tended to worsen at higher CM concentrations. Use of a minimum CM concentration based on the purpose of the examination and constant filling at the target region are effective for avoiding these artifacts.

1 Introduction

C-arm cone-beam computed tomography (CBCT) is a technique that reconstructs a three-dimensional (3D) image from a rotational scan by using the C-arm system [1]. This technique is useful for 3D image analysis in the diagnosis of aneurysm and vessel stenosis [2,3], in addition to evaluation by use of CT-like images of the perfusion area [4,5].

C-arm CBCT with a flat panel detector has higher spatial resolution, but has a number of disadvantages, such as lower dose efficiency, a smaller field of view, and lower temporal resolution, in comparison with the standard multi-slice CT. This type of system acquires all of the data in one scan over a period of a few seconds [6]. Therefore, there is a high probability that negative effects will occur in the scan volume with temporal changes in the patient during the scan. Inadequate breath holding or movement of body parts and of internal organs leads to motion artifacts due to inconsistent projection data [7].

Conventional digital subtraction angiography provides significant diagnostic value for the hemodynamic evaluation of the patient. C-arm CBCT allows 3D diagnosis, but is limited in static images. A dynamic change in a contrast medium (CM) can cause

inconsistent projection data in C-arm CBCT scans that use CM. Therefore, the target region needs to be filled uniformly by CM during the scan for accurate evaluation of the vessel form and the perfusion area. However, the arrival time of the injected CM is considered to differ depending on the injection protocol, the distance from the injection catheter, and the form of tissue [8]. Thus, the target region can potentially receive insufficient filling because of late arrival of CM.

We used a phantom to investigate the influence of insufficient filling during C-arm CBCT scans on image quality, which, to our knowledge, has not been reported on previously. We hypothesized that the results could be useful for determining the cause of artifacts observed incidentally in clinical examinations and for designing injection protocols.

2 Materials and methods

In this study, we used two methods to acquire images of CM arriving late during C-arm CBCT scans. The first method involved a simulation in which we scanned a phantom filled with different concentrations of CM and with water and then replaced the projection images partially between the different projection series. The second method

involved using an automatic power injector for injection of CM during scans.

2.1 Simulation method involving replacement of the projection images

In this method, we simulated CM filled into a vessel by replacing the projection images. This procedure allows elimination of experimental error and flexible construction of the intended projection data. All C-arm CBCT scans were performed on a C-arm angiography system (Artis zee ceiling-mounted system; Siemens AG, Forchheim, Germany) with a CsI amorphous silicon detector which has a pixel pitch of 154 μm. Projection images were acquired at a constant detector entrance dose (0.36 μGy/view) by automatic exposure control with use of the following parameters: tube voltage, 90 kVp; scan time, 8 s; total number of projection images, 396; projection image matrix, 616 × 480; angular scan range, 200°; fan angle, 18°; cone angle, 14°. We used iopamidol (Oypalomin 300; Fuji Pharma, Tokyo, Japan) as the target that simulated the vessel or the perfusion stain. A water- or CM-filled acrylic cylinder (internal diameter, 7 mm; external diameter, 9 mm) was inserted into the center hole of a 200-mm-diameter polyurethane cylindrical phantom (MHT type; Kyoto kagaku, Kyoto, Japan) that contained 13-mm-diameter holes at the center and at two peripheral points. This

phantom was fixed at the bed with vinyl tape and was located at the rotation center (Fig. 1a). Water or 100, 50, or 5% v/v concentration of CM in the phantom was scanned. These concentrations were selected based on previous studies demonstrating vessel [2], liver [4,5], and carotid artery with a stent [9]. In addition, we used an extension tube (internal diameter, 1.7 mm; Create Medic, Yokohama, Japan) with 100% v/v concentration of CM or water as the object for investigating artifacts generated as a function of target size. The positioning and scan conditions for this extension tube were the same as described above. We also investigated the positional dependence of the artifacts. The 7-mm-diameter 100% v/v CM- or water-filled phantom was located -80 mm along z-direction of the central hole (foot side) or the center of the top hole (top side) of the polyurethane cylindrical phantom, and scanned, respectively (Fig. 1b).

The acquired projection images were written to Digital Versatile Disc as Digital Imaging and Communications in Medicine files and imported to a personal computer. We used a binary editor (Stirling; available at http://www.vector.co.jp/soft/win95/util/se079072.html) to replace partially the front side of the projection series at each CM concentration with that of the projection series with water (Fig. 2). The projection series that contained 95, 90, 80, 70, 60, 50, 40, 30, 20, or 10% CM-filled projection images in the latter part of the projection series were

constructed by use of this process (Fig. 3). We define the percentage of CM-filled projection as follows,

$$\text{Percentage of CM - filled projection} = \frac{\text{the number of projection images containing CM}}{\text{total number of projection images}} \times 100. \quad (1)$$

Then, we imported the edited projection series to a postprocessing workstation (X Workplace; Siemens AG). The projection images imported to the workstation were confirmed to include the correct number of images and the required image quality. We used the following parameters to perform Feldkamp-type reconstructions [10]: slice matrix, 512 × 512; kernel type, “HU”; and image impression, “normal”; we then used a 1024 × 1024 matrix (0.26 mm/pixel) to reconstruct the 5-mm-thick axial images. The kernel type “HU” was designed to reconstruct the images proportional to X-ray absorption, and it had high density resolution. Therefore, we used this kernel for quantitative image evaluation. In the reconstruction process, the projection data were corrected by restoring of the linear relationship between the projection value and the X-ray path length through an assumed water-equivalent object in order to avoid beam hardening artifacts [11].

2.2 Injection study

The C-arm CBCT scan parameters were the same as those described in the previous section. Undiluted CM and water were placed in a dual-head power injector (Press DUO; Nemoto Kyorindo, Tokyo, Japan) and connected to a dual injection tube (Create Medic, Yokohama, Japan). The downstream side of the dual injection tube was connected to the extension tube (internal diameter, 1.7 mm) mentioned in the previous section, and this tube was passed through the central hole of the polyurethane cylindrical phantom. The tube was filled with CM until it reached the junction of the dual injection tube, and was filled with water until it reached the tube end.

The injection rate was 2 ml/s in all protocols, and only CM was injected. The injection protocols were as follows: the injection was started 4 s before the scan start (scan delay, 4 s), and the injection was started 0, 2, or 4 s after the scan start (injection delay, 0, 2, or 4 s). The experiment was repeated 3 times.

2.3 Image analysis

ImageJ software (available at http://rsb.info.nih.gov/ij/) was used for image analysis.

The average pixel value of a circular region of interest (ROI) of 4-mm diameter

centered in the CM area was measured in three consecutive slices for assessment of the lowering of pixel values due to insufficient CM filling. A circular ROI of 1-mm diameter was used for the extension tube.

For evaluating the distortion of the CM area, we created binary images with Image–Adjust–Threshold command as the threshold of the half value of the mean pixel value in the CM area and then used the Analyze–Analyze Particles command to determine the long and short axes of the CM area. Finally, we calculated the average long/short axis ratio in three consecutive slices.

The root mean square error (RMSE) between the axial image of perfect filling and that of insufficient filling was calculated by use of imageJ plug-in "SNR" (available from http://bigwww.epfl.ch/sage/soft/snr/) for evaluation of the differences of the artifacts. The RMSE is defined as follows,

$$RMSE = \sqrt{\frac{1}{n_x n_y} \cdot \sum_{0}^{n_x-1} \sum_{0}^{n_y-1} \left[r(x,y) - t(x,y) \right]^2} \qquad ,(2)$$

where $r(x,y)$ is the reference image (perfect filling), $t(x,y)$ is the test image (insufficient filling), and n is the matrix size.

We also evaluated the intensity profiles of the CM area for assessment of the cupping effect [12].

3 Results

3.1 Simulation method involving replacement of the projection images

Figure 4 shows the reconstruction of axial images of the undiluted 100% v/v concentration of CM. The percentages indicated in Fig. 4 represent the percentages of CM-filled projections. The “100%” value indicates that the projection images were not replaced. The image of 95% of the CM-filled projection shows no visible change in the CM area, but shows a slight streak artifact in the horizontal direction. The 90% image shows a streak artifact and a change in the circular shape of the CM area. The direction of the streak artifact changed clockwise, and the shape of the CM area changed elliptically with decreasing percentage of the CM-filled projection (in other words, with increased delay in CM arrival). In the axial images of the 1.7-mm-diameter CM-filled phantom, the dark and bright areas with streak artifacts were narrower than those in the 7-mm-diameter CM-filled phantom. The reconstructed axial images of 100, 50, and 5% v/v concentrations of CM at 50% of the CM-filled projection are shown in Fig. 4c. Strong streak artifacts that had large changes in the pixel values were observed at higher CM concentrations.

The average pixel values of the CM area decreased monotonically at each CM concentration (Fig. 5). The long/short axis ratios of the CM area for 100, 50, and 5% v/v concentrations are shown in Fig. 6.

The long/short axis ratio of the 7-mm-diameter phantom increased with decreasing percentage of the CM-filled projection and decreased after peaking at 40% for any CM concentration. The long/short axis ratio tended to be higher at higher CM concentrations at <60% of the CM-filled projection. In the long/short axis ratio of the 1.7-mm-diameter phantom, the distortion tendencies were approximately similar, except for the amplitude.

RMSEs of the axial images for 100, 50, and 5% v/v concentrations are shown in Fig. 7. The RMSE increased with decreasing percentage of the CM-filled projection, and was higher at higher concentrations of CM. The increasing rate of the RMSE of the 1.7-mm-diameter phantom was very much slower than that of the 7-mm-diameter phantom.

The intensity profiles of the CM area in Fig. 4a,c are shown in Fig. 8. The lower portion of the profiles was observed, and this portion became lower with decreasing percentages of the CM-filled projection. The higher concentration of CM also decreased the pixel value in the central portion of the CM.

Figure 9 shows the pixel values, RMSE, and the long/short axis ratios in comparison with different positions of the CM-filled phantom. Slight differences of the pixel values were observed at a lower percentage of the CM-filled projection. The RMSE of the foot side was slightly higher than that of the center at a lower percentage of the CM-filled projection, and the RMSE of the top side was lower than that of the center at <70% of the CM-filled projection. There was no significant difference in the long/short axis ratios.

3.2 Injection study

The axial images scanned in each scan delay and injection delay time are shown in Fig. 10. The axial images at a scan delay of 4 s had no visible artifacts and had a circular CM area because of CM arrival before the scan start (Fig. 10a). The axial images for cases in which the CM arrived after the scan start (injection delay, 0, 2, or 4 s) had streak artifacts, with an elliptical CM area (Fig. 10b–d). The direction of the streak artifacts was changed, and the CM area was distorted strongly with increasing delay in CM arrival, as was the case in the simulation method. The average pixel values of the CM area were 7034 ± 38 (mean ± SD), 5827 ± 55, 3936 ± 29, and 1849 ± 47 in the order of

earliest to latest arrival time. The long/short axis ratios were 1.09 ± 0.08, 1.31 ± 0.06, 2.07 ± 0.07, and 2.69 ± 0.05.

4 Discussion

Our study showed that streak artifacts and distortion of the CM area were observed in the images when the CM concentration during the C-arm CBCT scan was changed rapidly. These artifacts were considered to be caused by inconsistent projection associated with dynamically changing CM.

The direction of the streak artifacts changed depending on the arrival time of the CM, and the streak artifact was stronger at higher CM concentrations. Such strong artifacts could lead to difficulties in assessment of the target vessel and perfusion area. Distortion of the CM area could also prevent accurate diagnosis. This distortion increased with increasing inconsistency of projection. Furthermore, the relative distortion was larger at smaller target sizes; therefore, the measurement error would be large at targets, such as small vessels with insufficient CM-filling data.

The variation in the RMSE which represents the total amount of artifacts increases depending on the higher concentration of CM and filling insufficiency (Fig. 7). In

addition, the lower portion of the intensity profiles represents the cupping effect based on beam hardening, and this cupping effect is also worse, depending on the same factors.

The C-arm CBCT technique requires high-contrast images of undiluted CM for evaluation of a vessel [2], but evaluation of the perfusion area requires images of diluted CM [4,5]. If insufficient filling occurs during the scan, high CM concentrations not only cause beam-hardening artifacts [13], but also have a high probability of generating strong streak artifacts and distortion, as described above. Therefore, it is desirable to use diluted CM except in cases in which especially high contrast is needed. In general, although the target area is unlikely to show insufficient filling during scanning at the time the CM reaches the target area, the area distal from the target tends to be filled insufficiently because the CM arrives later there than at the target area. However, artifacts in the distal area would not be likely to be observed because the dilution effect is higher distally than proximally.

As Fig. 9 a shows, the pixel value at the center is lower than that of the periphery; this would be due to an increasing out-of-plane scatter contribution [14]. The RMSE of the top side decreased because the area affected by streak artifacts is limited by the position of the CM in the phantom.

The phantom we used in this study was uniform in composition; however, an object in clinical case is uniformity and not a circular shape. Therefore, in clinical examinations, the inconsistency of the projection data could be higher due to the variation of the transmission through the object. Moreover, as distinct from this study, there is a probability of the existence of a number of CM areas in and out of the field of view in a clinical object. In such cases, the influence of beam hardening and scatter is higher. As a result, the variation of pixel values, the cupping effect, and streak artifacts could be high.

Acquired images showed the decreasing pixel value and distortion in the CM area in the injection study as well as in the simulation. However, the streak artifacts were less visible in the injection study than with the simulation method, which might be caused by the discontinuities resulting from changes in the CM with the simulation method. Therefore, the streak artifacts could depend on the change in the CM concentration per time. The percentages of the CM-filled projections were 83, 62, and 32% for injection delays of 0, 2, and 4 s, respectively; these percentages were determined by analysis of the projection images in the injection study. The directions of the streak artifacts in these axial images in the injection study (Fig. 10b-d) were almost the same as those in the 80, 60, and 30% projections (Fig. 4b), used in the simulation method. The

tendencies toward decreasing pixel values and increasing distortion were also the same as those observed with the simulation method (Fig. 11), which validated the simulation method. Moreover, although we did not demonstrate washout by blood flow after stopping the injection in this experiment, injection of a small amount of CM in short times in a clinical examination could cause a similar artifact because of inconsistent projection in the later part of the scan.

Even if the CM arrives before the scan start, an intricately shaped object such as a cerebral aneurysm has the probability of insufficient filling. There was a report that an initial bolus with a two-phase injection technique improved the filling of a cerebral aneurysm model, in comparison with the continuous-flow technique [15]. A saline flush generally improves the late of time-intensity profile. Therefore, various injection techniques, including a variable injection rate, should be considered for uniform filling of the target in a clinical case.

Figures 4 and 10b show approximately 20% delay in CM arrival relative to the total scan time, which resulted in obvious distortion of the filling area. To avoid such artifacts, injection protocols should specify that most of the CM has arrived at the target region at the start of scanning. On the other hand, the frequency of contrast-induced acute kidney injury has been shown to be associated with an increasing CM volume [16]; therefore,

the CM volume should be minimized as much as possible. Optimal dilution of CM based on the purpose of the examination [9,17] should reduce CM volumes and avoid these artifacts.

5 Conclusion

Our study indicated that insufficient CM filling during C-arm CBCT scans causes decreased pixel values and increased distortion of the CM area, in addition to streak artifacts. Use of a minimum CM concentration based on the purpose of the examination and constant filling of the CM at the target region are important for avoiding these artifacts.

References

1. Siewerdsen JH. Cone-Beam CT with a Flat-Panel Detector: From Image Science to Image-Guided Surgery. Nucl Instrum Methods Phys Res A. 2011;648:S241-50.

2. Li J, Wan F, Chen G, Ma L, Zhang G, Xu G, Gong J. The utility of angiographic CT in the diagnosis and treatment of neurovascular pathologies in the vicinity of cranial base. Neurosurg Rev. 2010;34:243-8.

3. Patel NV, Gounis MJ, Wakhloo AK, Noordhoek N, Blijd J, Babic D, Takhtani D, Lee SK, Norbash A. Contrast-enhanced angiographic cone-beam CT of cerebrovascular stents: experimental optimization and clinical application. AJNR Am J Neuroradiol. 2011;32:137-44.

4. Miyayama S, Yamashiro M, Okuda M, Yoshie Y, Nakashima Y, Ikeno H, Orito N, Matsui O. Detection of corona enhancement of hypervascular hepatocellular carcinoma by C-arm dual-phase cone-beam CT during hepatic arteriography. Cardiovasc Intervent Radiol. 2011;34:81-6.

5. Koelblinger C, Schima W, Berger-Kulemann V, Wolf F, Plank C, Weber M, Lammer J. C-arm CT during hepatic arteriography tumour-to-liver contrast: intraindividual comparison of three different contrast media application protocols. Eur Radiol. 2013;23:938-42.

6. Kalender WA, Kyriakou Y. Flat-detector computed tomography (FD-CT). Eur Radiol. 2007;17:2767-79.

7. Marchant TE, Price GJ, Matuszewski BJ, Moore CJ. Reduction of motion artefacts in on-board cone beam CT by warping of projection images. Br J Radiol. 2011;84:251-64.

8. Bash S, Villablanca JP, Jahan R, Duckwiler G, Tillis M, Kidwell C, Saver J, Sayre J. Intracranial vascular stenosis and occlusive disease: evaluation with CT angiography,

MR angiography, and digital subtraction angiography. AJNR Am J Neuroradiol. 2005;26:1012-21.

9. Hosokawa S, Kawai N, Sato M, Minamiguchi H, Nakai M, Nishioku T, Sonomura T, Matsumoto H, Masuo O, Itakura T. Optimal contrast material concentration for distinguishing among carotid artery lumen, carotid stent, and neck in cone-beam computed tomography during carotid angiography: basic and clinical studies. Jpn J Radiol. 2012;30:358-64.

10. Feldkamp LA, Davis LC, Kress JW. Practical cone-beam algorithm. J Opt Soc Am. 1984;A1:612-19.

11. Zellerhoff M, Scholz B, Ruehrnschopf EP, Brunner B. Low contrast 3D reconstruction from C-arm data. Proc SPIE. 2005;5745:646-55.

12. Hunter AK, McDavid WD. Characterization and correction of cupping effect artefacts in cone beam CT. Dentomaxillofac Radiol. 2012;41:217-23.

13. Loffroy R, Lin M, Rao P, Bhagat N, Noordhoek N, Radaelli A, Blijd J, Geschwind JF. Comparing the detectability of hepatocellular carcinoma by C-arm dual-phase cone-beam computed tomography during hepatic arteriography with conventional contrast-enhanced magnetic resonance imaging. Cardiovasc Intervent Radiol. 2012;35:97-104.

14. Orth RC, Wallace MJ, Kuo MD. C-arm cone-beam CT: general principles and technical considerations for use in interventional radiology. J Vasc Interv Radiol. 2008;19:814-20.

15. Ernemann UU, Gronewaller E, Duffner FB, Guervit O, Claassen J, Skalej MD. Influence of geometric and hemodynamic parameters on aneurysm visualization during three-dimensional rotational angiography: an in vitro study. AJNR Am J Neuroradiol. 2003;24:597-603.

16. Brown JR, Robb JF, Block CA, Schoolwerth AC, Kaplan AV, O'Connor GT, Solomon RJ, Malenka DJ. Does safe dosing of iodinated contrast prevent contrast-induced acute kidney injury? Circ Cardiovasc Interv. 2010;3:346-50.

17. Ritter M, Weiss C, Rassweiler MC, Michel MS, Hacker A. Optimizing imaging quality in endourology with the Uro Dyna-CT: contrast agent dilution matters. World J Urol. 2012 (epub).

Figure captions

Fig. 1

(a) Schematic of the polyurethane cylindrical phantom positioned at the rotation center

of the C-arm CBCT system. Arrow indicates C-arm 200° rotational scans. (b) Cross-sectional view of the polyurethane cylindrical phantom (upper) and the 7-mm-diameter and the 1.7-mm-diameter CM- or water-filled phantom (lower). The 7-mm-diameter 100% v/v CM- or water-filled phantom was located as shown in this illustration.

Fig. 2

Outline drawing representing the scheme for replacing the projection images between the projection series of the CM- and the water-filled phantom.

Fig. 3

Example showing the constitution of the created projection series. The ordinate represents the CM concentration, and the abscissa represents the percentage of projection.

Fig. 4

Reconstructed axial images of 100, 95, 90, 80, 70, 60, 50, 40, 30, 20, and 10% of projections of the undiluted 100% v/v concentration of CM in (a) the 7-mm-diameter

phantom and (b) the 1.7-mm-diameter phantom. (c) Reconstructed axial images of 100, 50, and 5% v/v concentrations of CM in the 50% of CM-filled projection.

Fig. 5

Variation in the pixel values of the CM-filling area as a function of the percentage of the CM-filled projection for 100, 50, and 5% v/v concentrations of CM.

Fig. 6

The long/short axis ratio of the CM area as a function of the percentage of the CM-filled projection for 100, 50, and 5% v/v concentrations of CM in the 7-mm-diameter phantom, and for 100% v/v concentration in the 1.7-mm-diameter phantom.

Fig. 7

RMSE of the axial images as a function of the percentage of the CM-filled projection for 100, 50, and 5% v/v concentrations of CM in the 7-mm-diameter phantom, and for 100% v/v concentration in the 1.7-mm-diameter phantom.

Fig. 8

(a) Intensity profiles of the CM area of 100% v/v concentration of CM for 100, 70, 50, and 20% of CM-filled projection. (b) The intensity profiles of 50% of CM-filled projection for 100, 50, and 5% v/v concentrations of CM. The intensities were normalized by each peak intensity.

Fig. 9

(a) The pixel values, (b) RMSE, and (c) long/short axis ratio as a function of the percentage of the CM-filled projection in comparison with different positions of the CM-filled phantom.

Fig. 10

Axial images acquired in the injection study at a (a) scan delay of 4 s and injection delays of (b) 0 s, (c) 2 s, and (d) 4 s.

Fig. 11

The long/short axis ratio of the CM area in the extension tube compared between the simulation method and the injection study.

Fig. 1 a

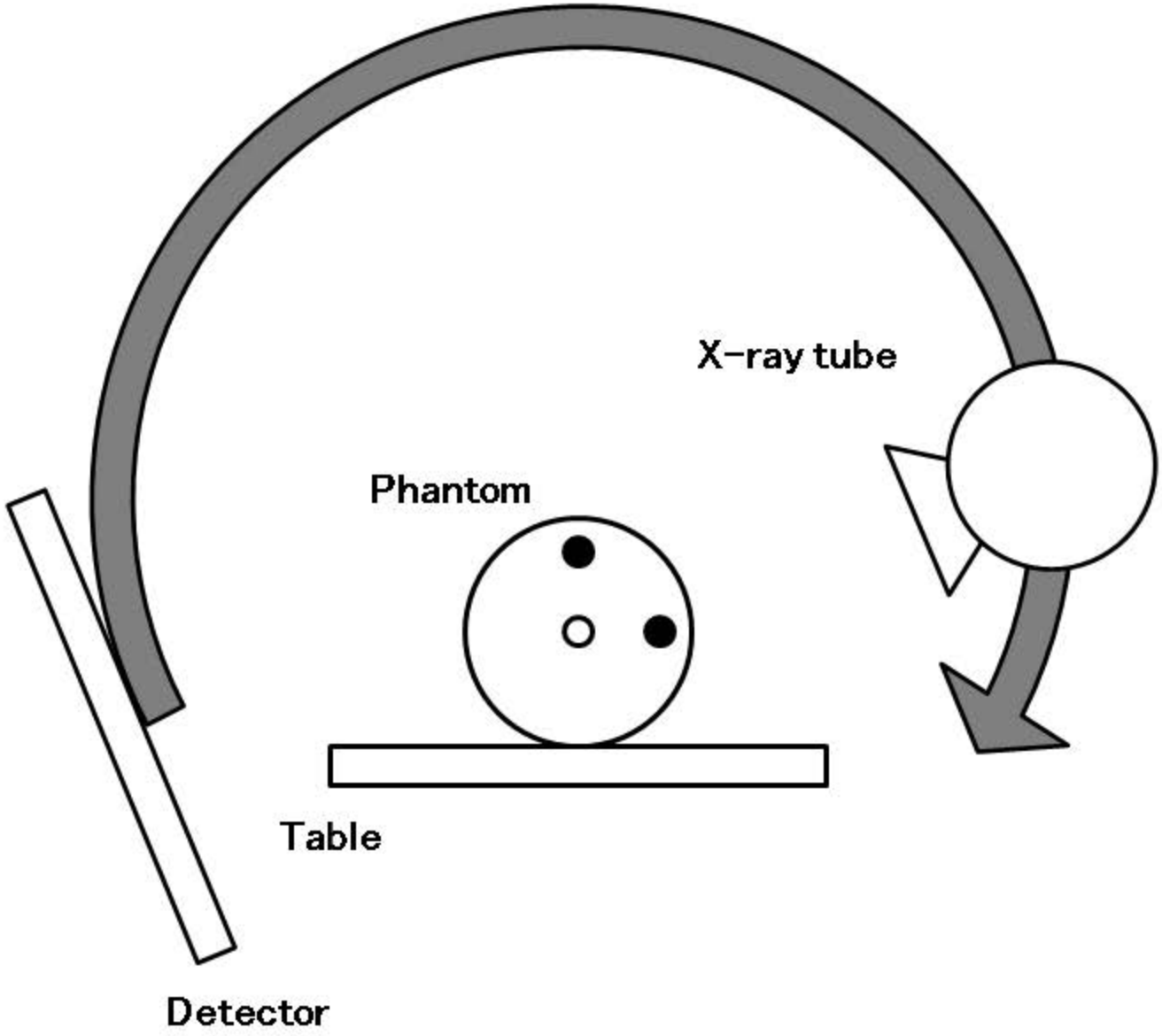

Fig. 1 b

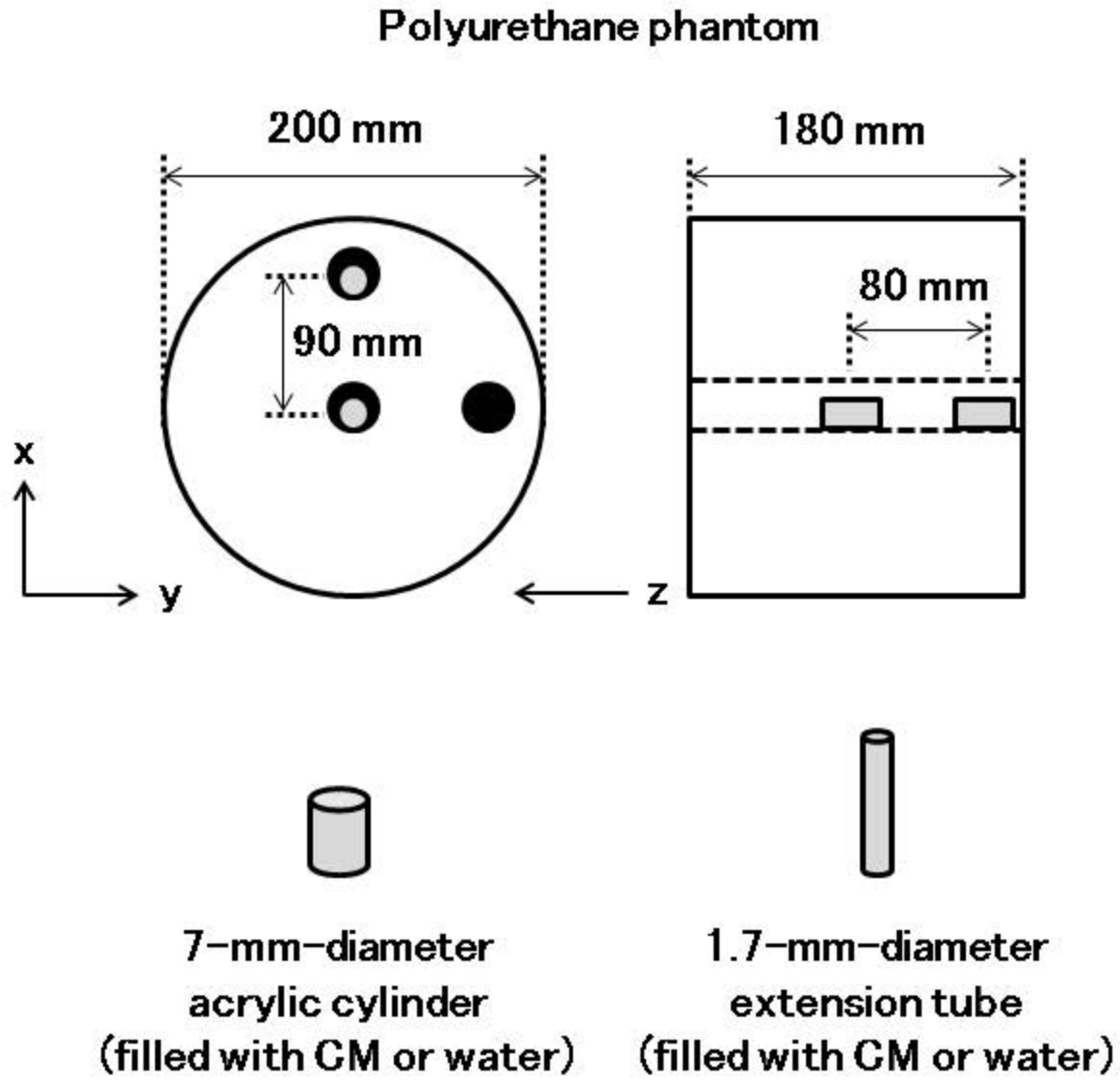
Polyurethane phantom
200 mm
180 mm
80 mm
90 mm
x
y
z
7-mm-diameter
acrylic cylinder
(filled with CM or water)
1.7-mm-diameter
extension tube
(filled with CM or water)

Fig. 2

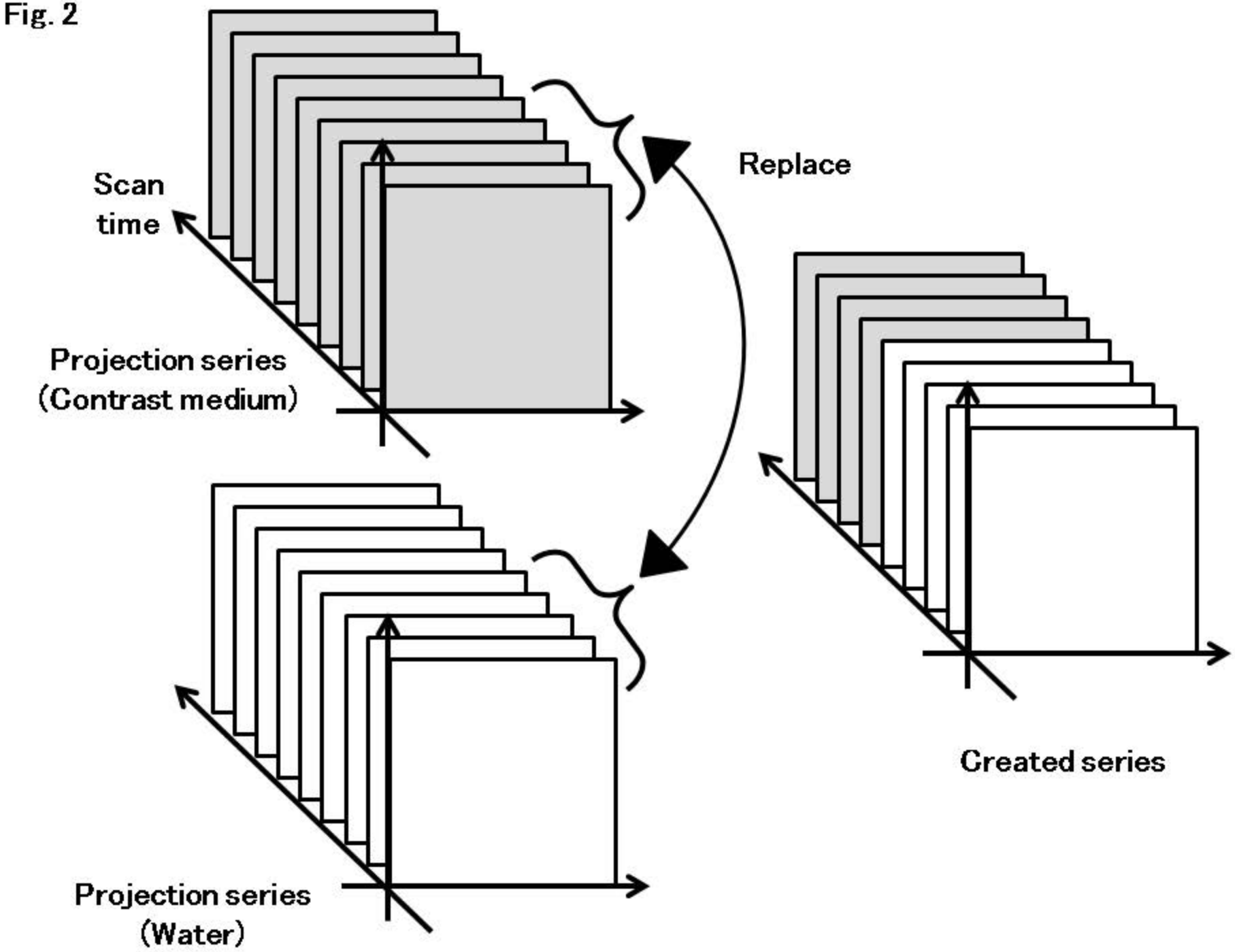
Scan
time
Projection series
(Contrast medium)
Replace
Created series
Projection series
(Water)

Fig. 3

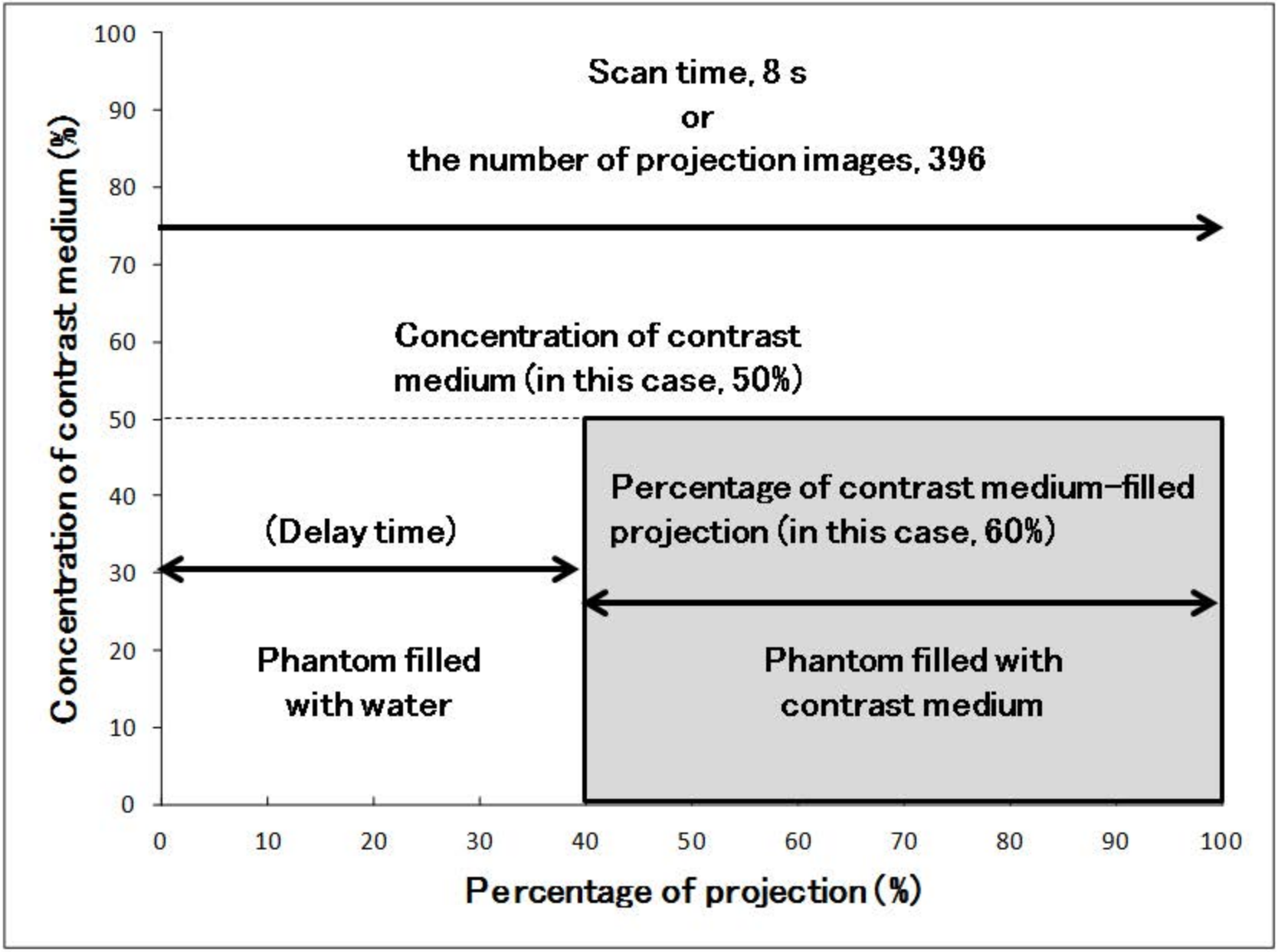
Scan time, 8 s
or
the number of projection images, 396
Concentration of contrast medium (in this case, 50%)
Percentage of contrast medium-filled projection (in this case, 60%)
(Delay time)
Phantom filled with water
Phantom filled with contrast medium
Concentration of contrast medium (%)
Percentage of projection (%)
0
10
20
30
40
50
60
70
80
90
100

Fig. 4

(a)

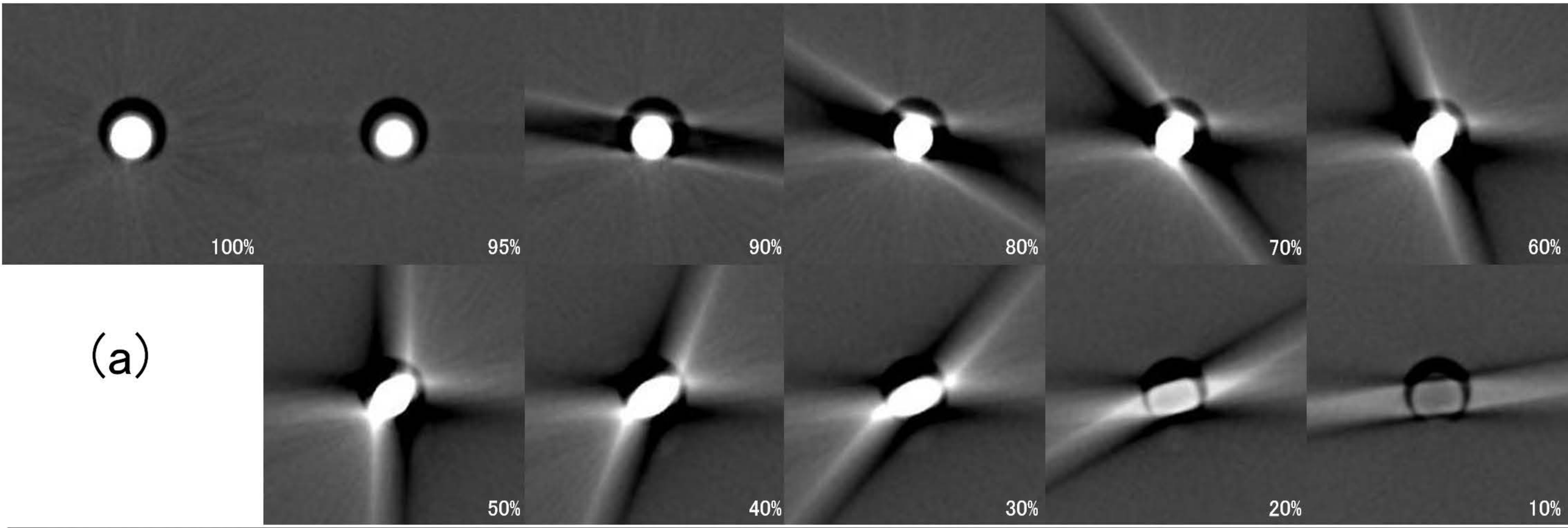
100%
95%
90%
80%
70%
60%
50%
40%
30%
20%
10%

(b)

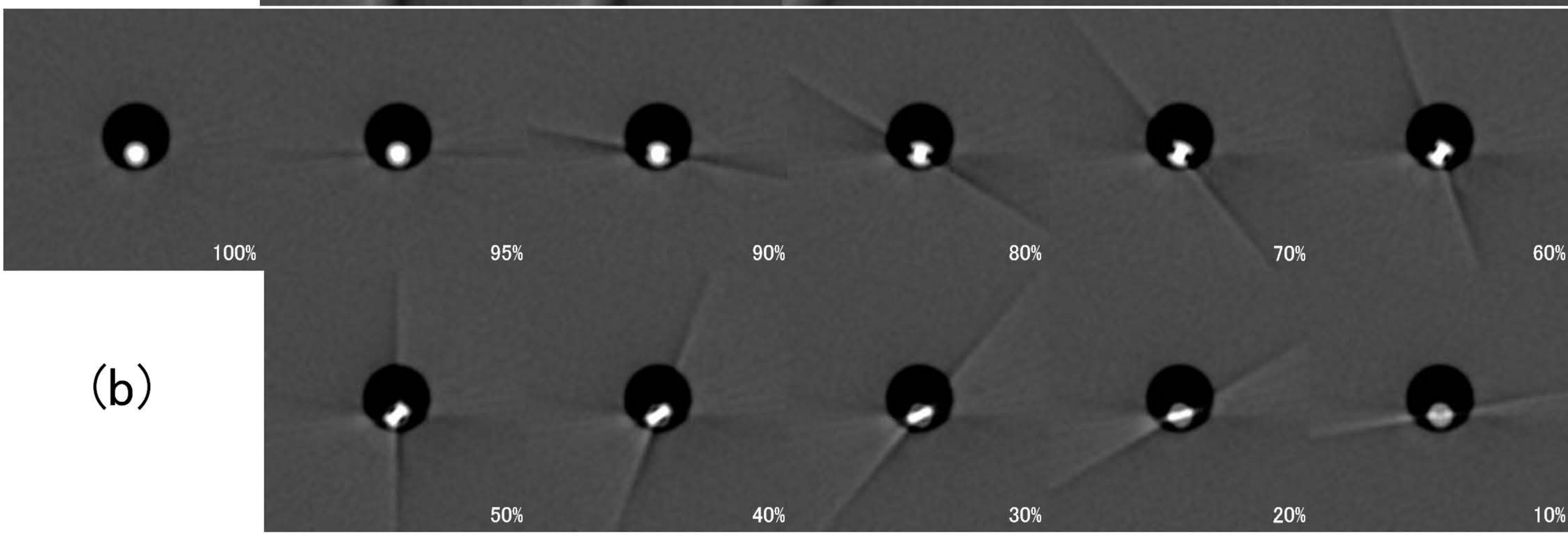
100%
95%
90%
80%
70%
60%
50%
40%
30%
20%
10%

(c)

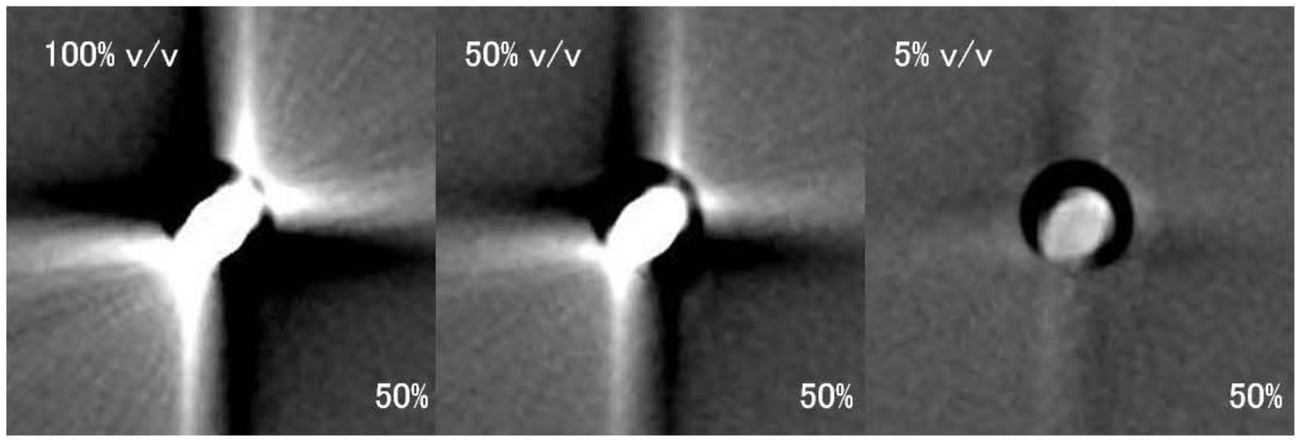
100% v/v
50%
50% v/v
50%
5% v/v
50%

Fig. 5

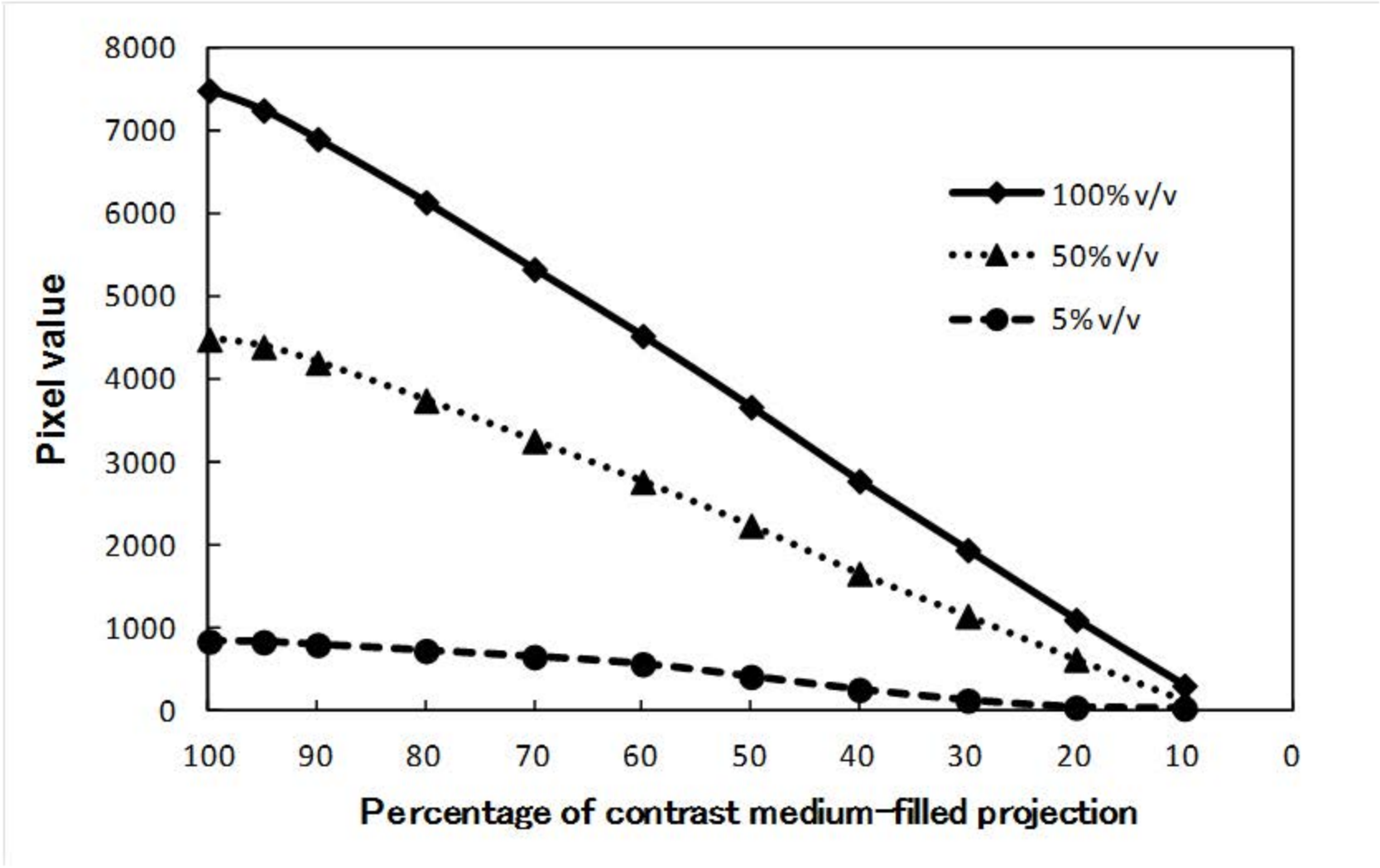
8000
7000
6000
5000
4000
3000
2000
1000
0
Pixel value
100
90
80
70
60
50
40
30
20
10
0
Percentage of contrast medium-filled projection
100% v/v
50% v/v
5% v/v

Fig. 6

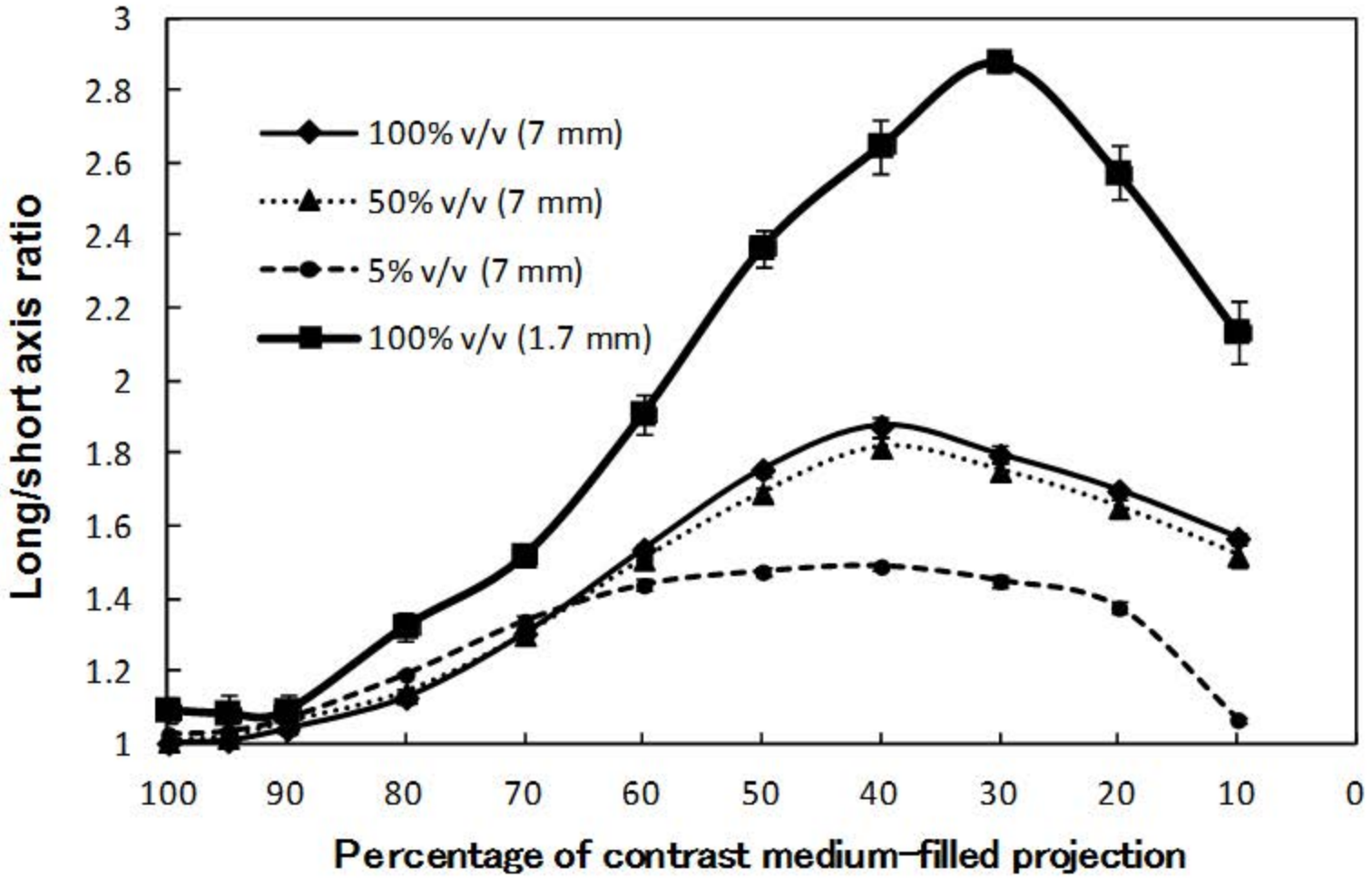
Long/short axis ratio
3
2.8
2.6
2.4
2.2
2
1.8
1.6
1.4
1.2
1
100% v/v (7 mm)
50% v/v (7 mm)
5% v/v (7 mm)
100% v/v (1.7 mm)
100
90
80
70
60
50
40
30
20
10
0
Percentage of contrast medium-filled projection

Fig. 7

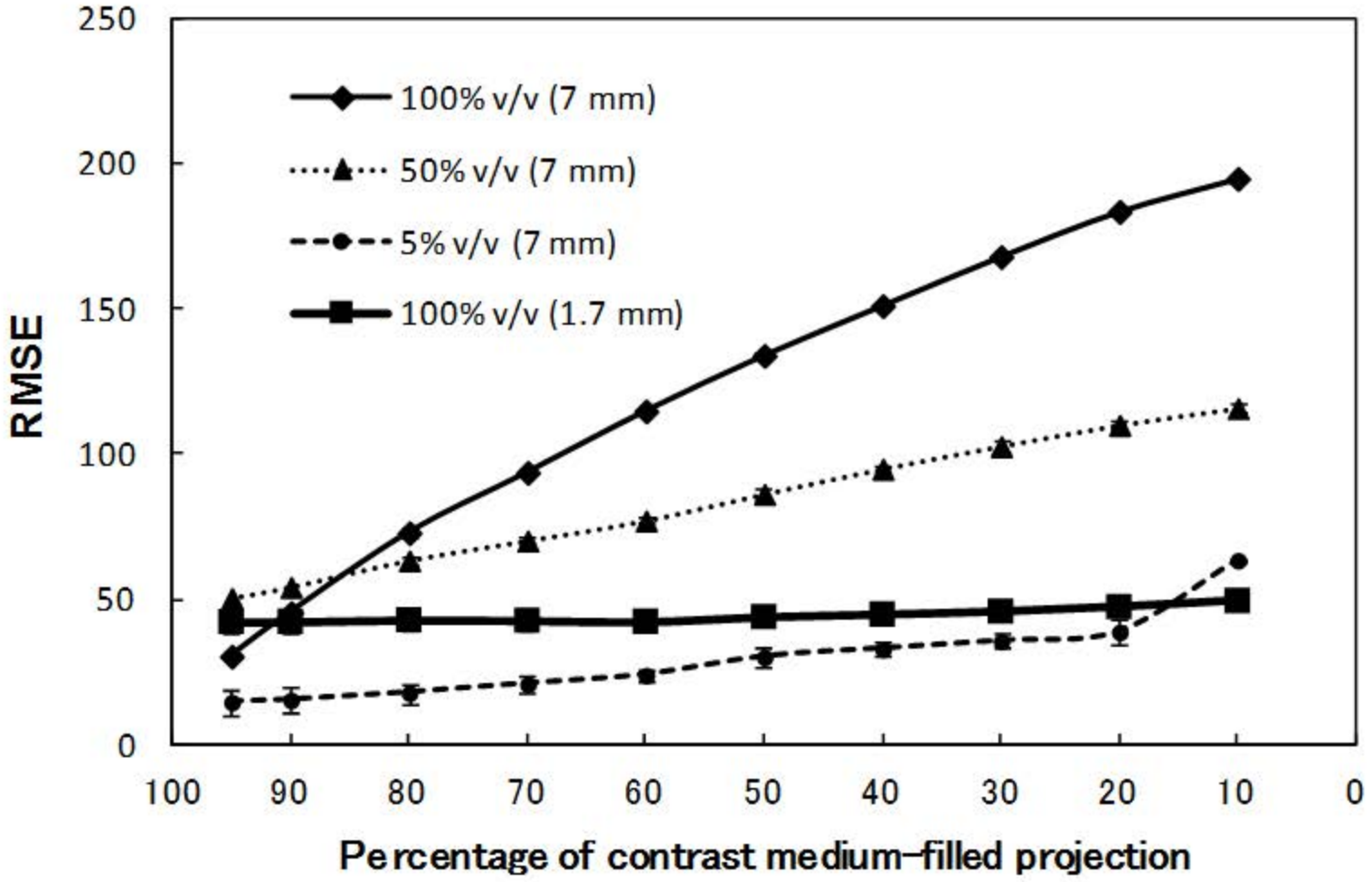
250
200
150
100
50
0
RMSE
100% v/v (7 mm)
50% v/v (7 mm)
5% v/v (7 mm)
100% v/v (1.7 mm)
100
90
80
70
60
50
40
30
20
10
0
Percentage of contrast medium-filled projection

Fig. 8 a

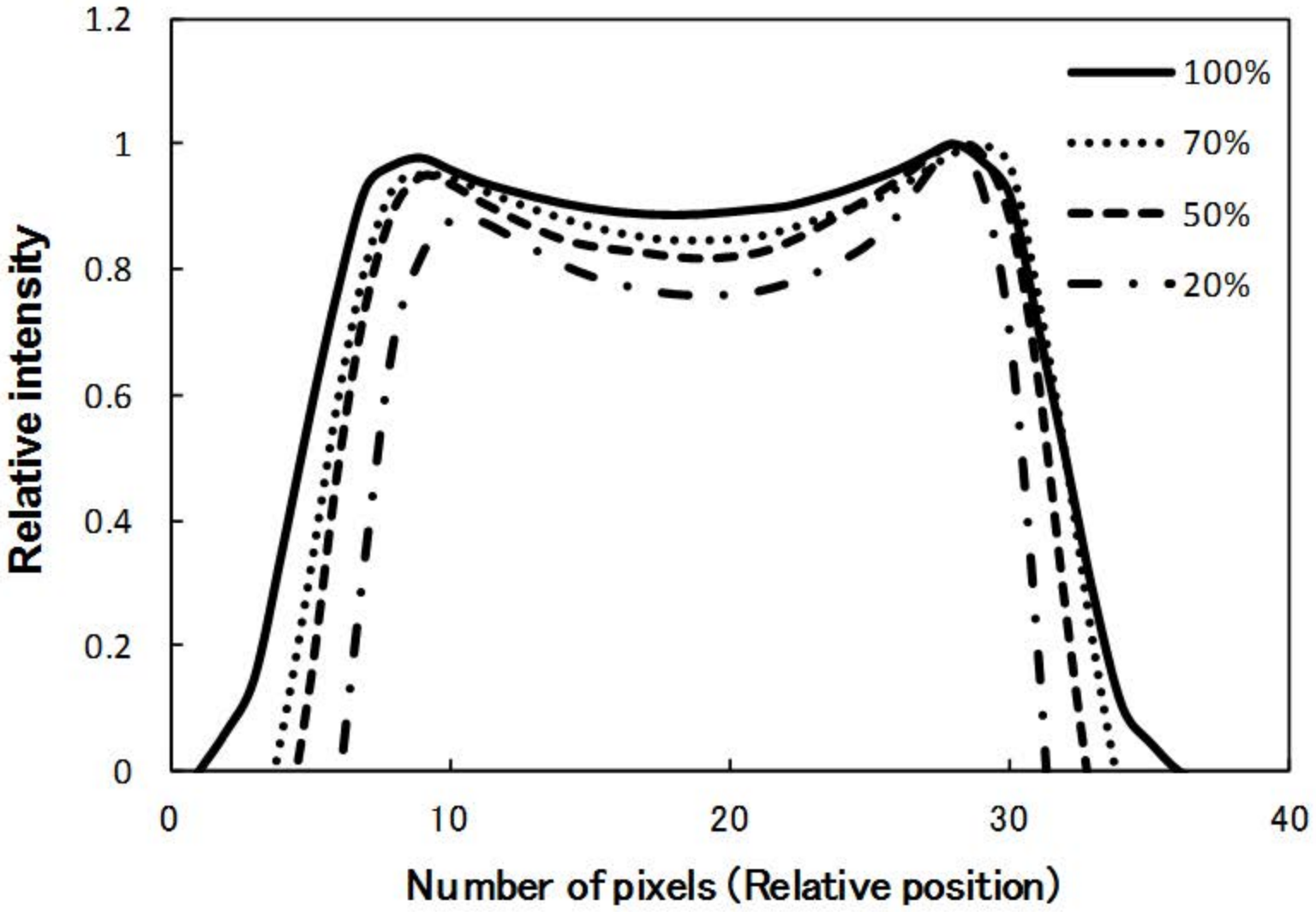
1.2
1
0.8
0.6
0.4
0.2
0
Relative intensity
0
10
20
30
40
Number of pixels (Relative position)
100%
70%
50%
20%

Fig. 8 b

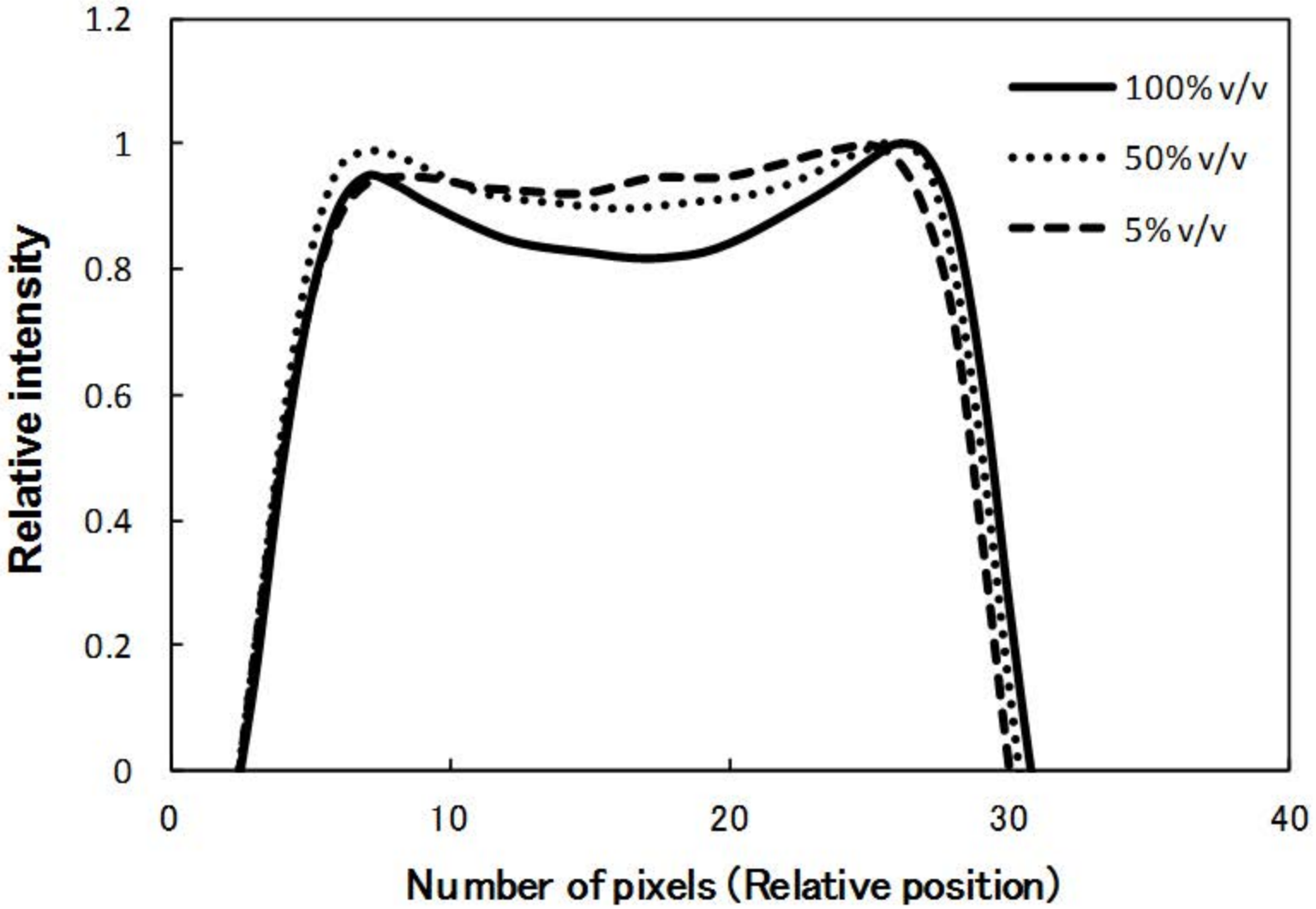
1.2
1
0.8
0.6
0.4
0.2
0
Relative intensity
0
10
20
30
40
Number of pixels (Relative position)
100% v/v
50% v/v
5% v/v

Fig. 9 a

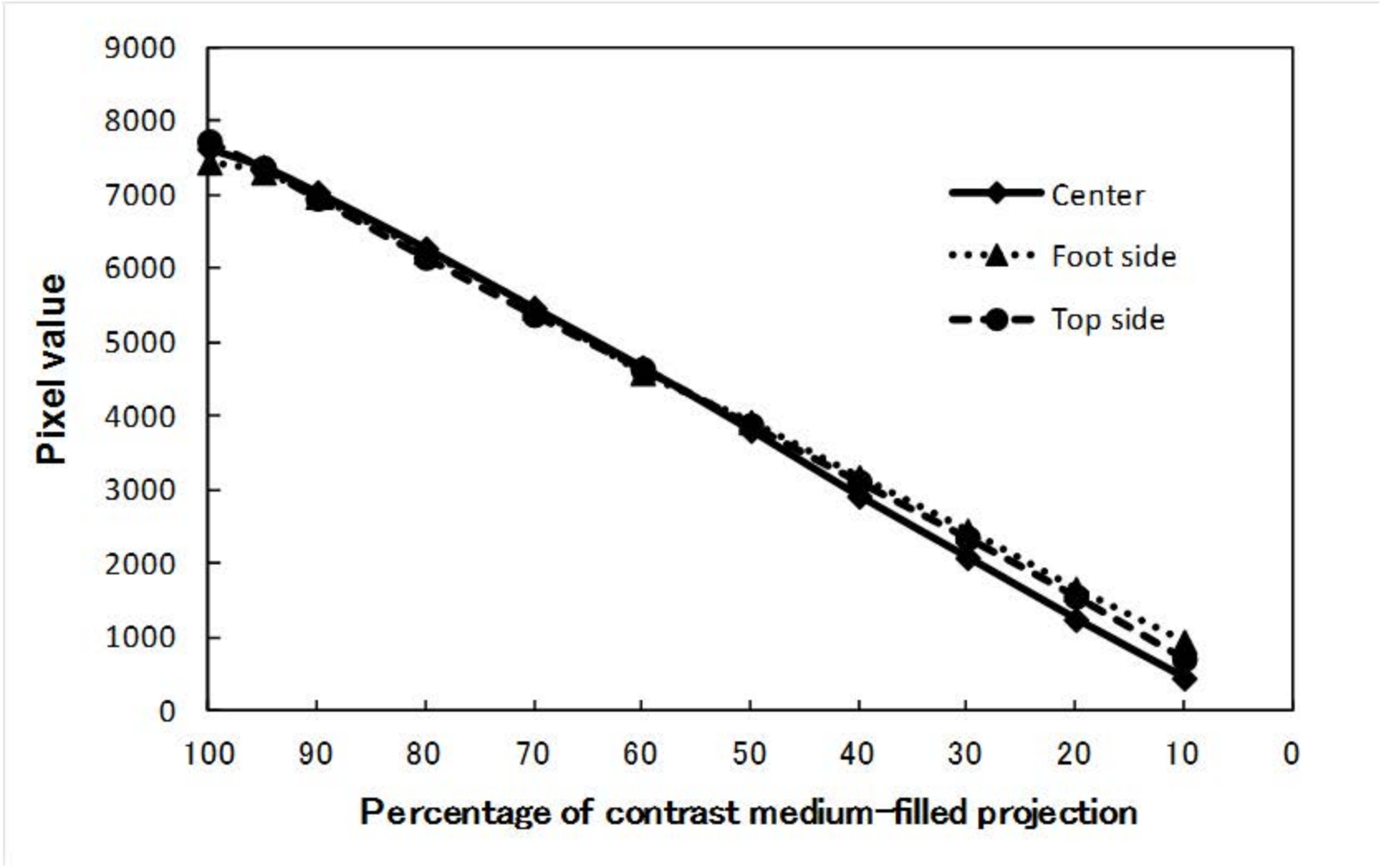
9000
8000
7000
6000
5000
4000
3000
2000
1000
0
Pixel value
100
90
80
70
60
50
40
30
20
10
0
Percentage of contrast medium-filled projection
Center
Foot side
Top side

Fig. 9 b

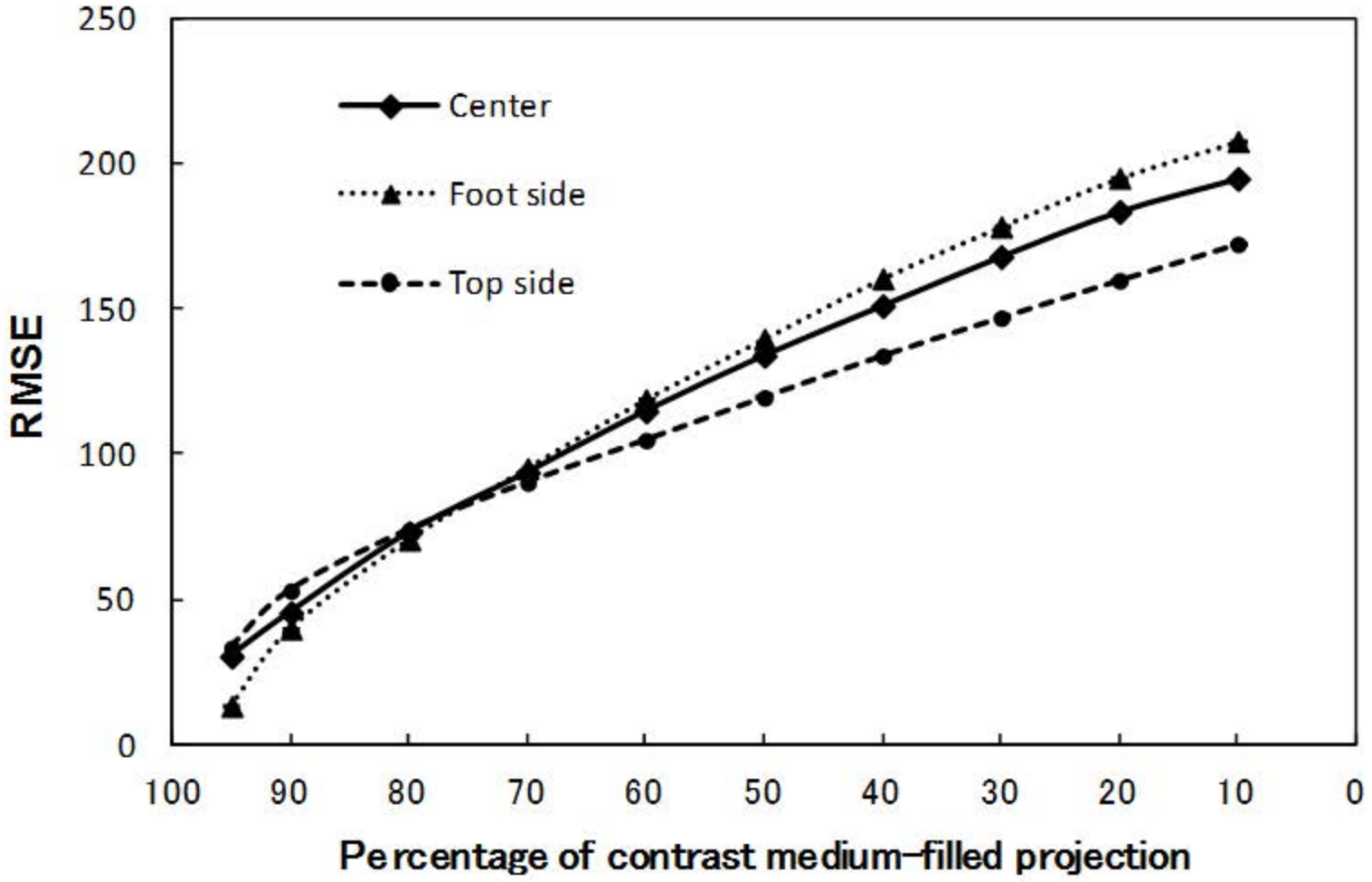
250
200
150
100
50
0
RMSE
Center
Foot side
Top side
100
90
80
70
60
50
40
30
20
10
0
Percentage of contrast medium-filled projection

Fig. 9 c

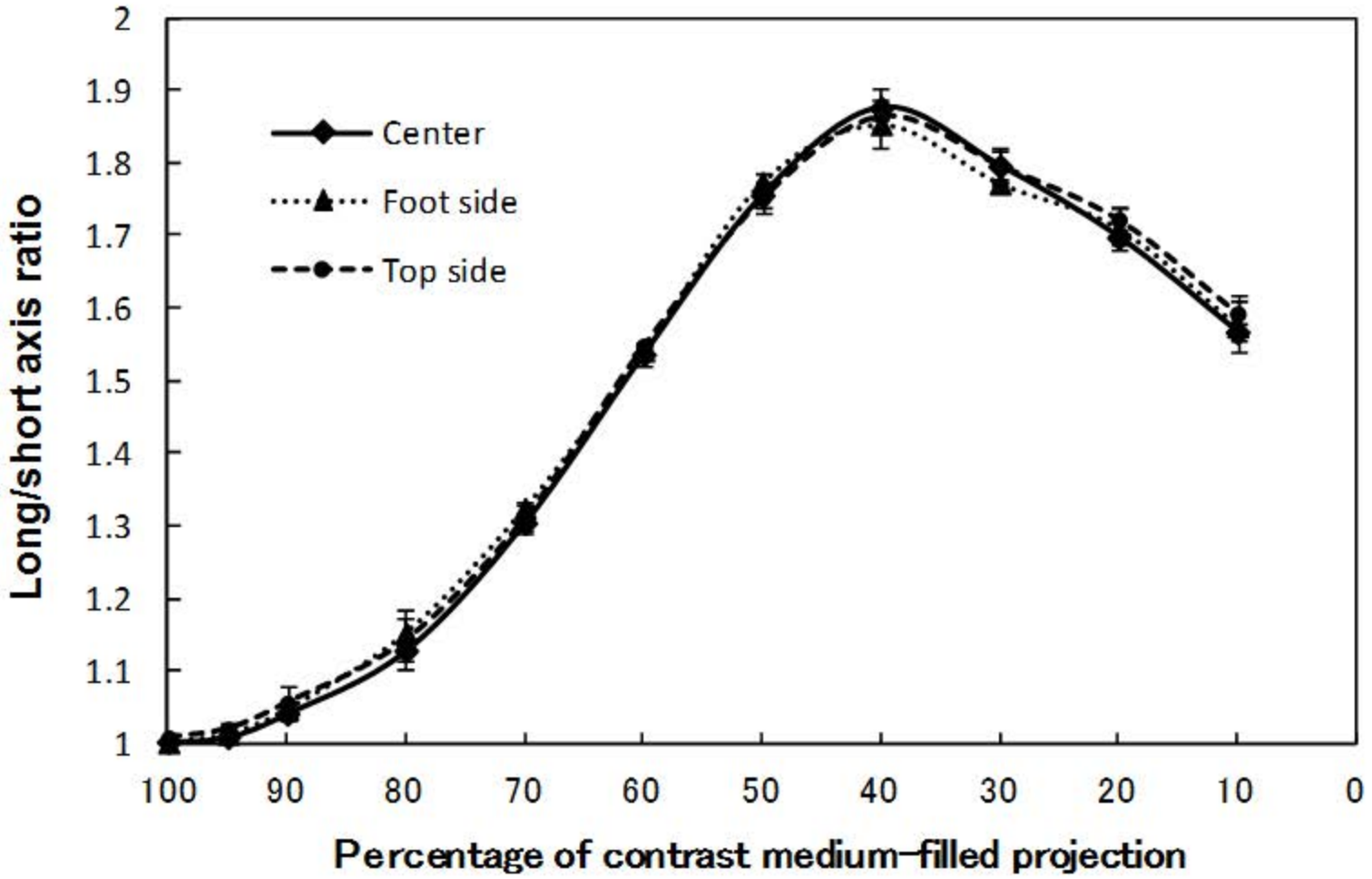
Long/short axis ratio
2
1.9
1.8
1.7
1.6
1.5
1.4
1.3
1.2
1.1
1
Center
Foot side
Top side
100
90
80
70
60
50
40
30
20
10
0
Percentage of contrast medium-filled projection

Fig. 10

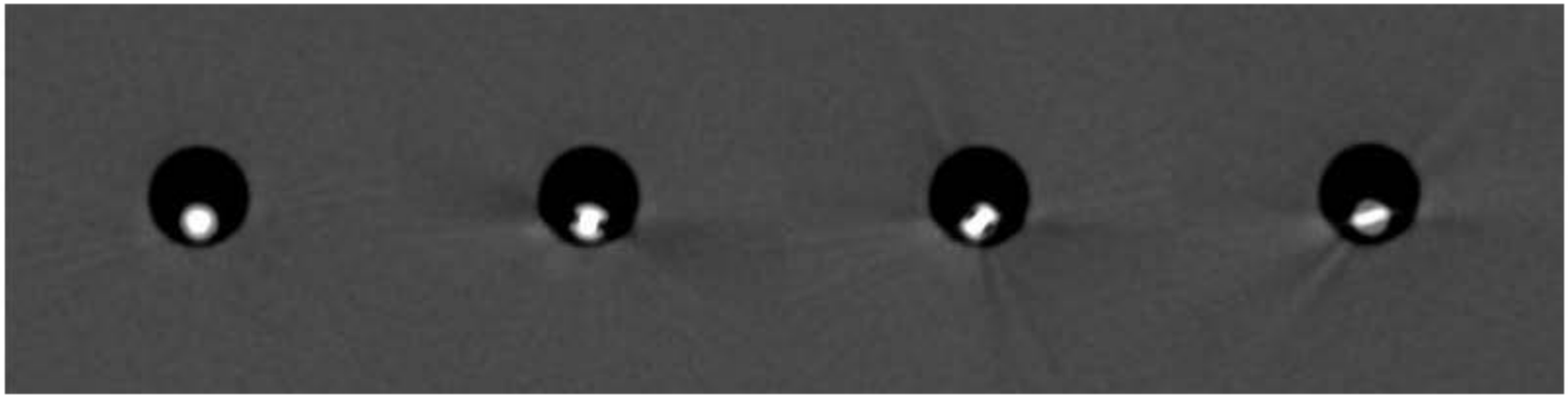

(a) (b) (c) (d)

Fig. 11

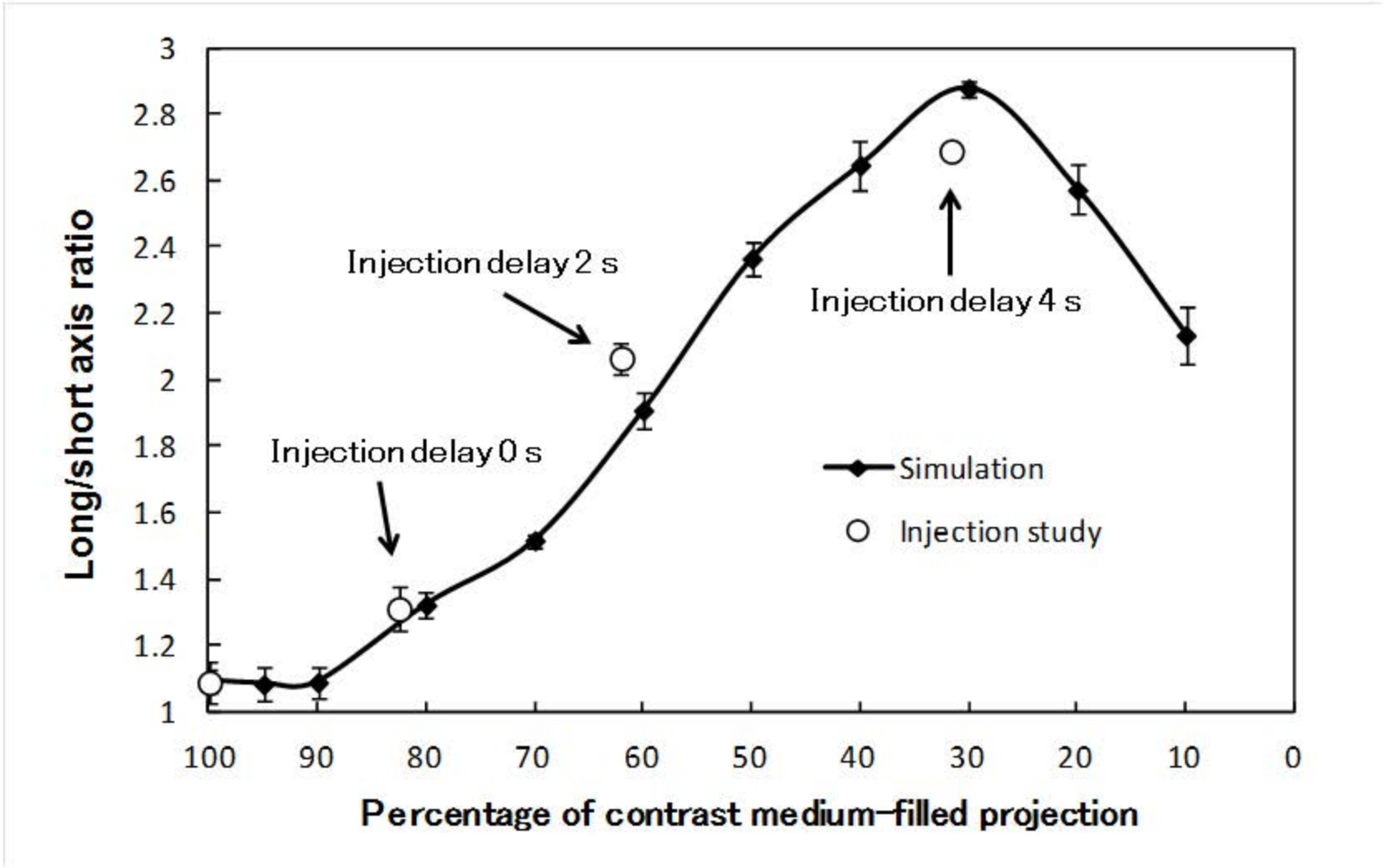
Long/short axis ratio
3
2.8
2.6
2.4
2.2
2
1.8
1.6
1.4
1.2
1
100
90
80
70
60
50
40
30
20
10
0
Percentage of contrast medium-filled projection
Injection delay 2 s
Injection delay 4 s
Injection delay 0 s
Simulation
Injection study